

Effect of copper/tungsten heterophase interface on radiation resistance: Insights from atomistic simulations

Wen Chen(陈文), Min Li(李敏), Bao-Qin Fu(付宝勤), Tun Chen(陈暾), Jie-Chao Cui(崔节超), and Qing Hou(侯氢)
Citation : Chin. Phys. B, 2025, 34 (**4**): 046108. DOI: 10.1088/1674-1056/adb40d
Journal homepage: http://cpb.iphy.ac.cn; http://iopscience.iop.org/cpb

What follows is a list of articles you may be interested in

Molecular dynamics simulations of collision cascades in polycrystalline tungsten

Lixia Liu(刘丽霞), Mingxuan Jiang(蒋明璇), Ning Gao(高宁), Yangchun Chen(陈阳春), Wangyu Hu(胡望宇), and Hiuqiu Deng(邓辉球)
Chin. Phys. B, 2025, 34 (**4**): 046103. DOI: 10.1088/1674-1056/adb410

Atomic origin of minor alloying element effect on glass forming ability of metallic glass

Shan Zhang(张珊), Qingan Li(李庆安), Yong Yang(杨勇), and Pengfei Guan(管鹏飞)
Chin. Phys. B, 2025, 34 (**3**): 036105. DOI: 10.1088/1674-1056/ada756

Exploring superconductivity in dynamically stable carbon-boron clathrates trapping molecular hydrogen

Akinwumi Akinpelu, Mangladeep Bhullar, Timothy A. Strobel, and Yansun Yao
Chin. Phys. B, 2025, 34 (**3**): 036103. DOI: 10.1088/1674-1056/ada757

Structural and transport properties of $(Mg,Fe)SiO_3$ at high temperature and high pressure

Shu Huang(黄澍), Zhiyang Xiang(向志洋), Shi He(何适), Luhan Yin(尹路寒), Shihe Zhang(张时赫), Chen Chen(陈晨), Kaihua He(何开华), and Cheng Lu(卢成)
Chin. Phys. B, 2025, 34 (**3**): 036102. DOI: 10.1088/1674-1056/ada759

Quasi-plastic deformation mechanisms and inverse Hall-Petch relationship in nanocrystalline boron carbide under compression

Zhen Yue(岳珍), Jun Li(李君), Lisheng Liu(刘立胜), and Hai Mei(梅海)
Chin. Phys. B, 2024, 33 (**8**): 086105. DOI: 10.1088/1674-1056/ad4989

Effect of copper/tungsten heterophase interface on radiation resistance: Insights from atomistic simulations

Wen Chen(陈文), Min Li(李敏), Bao-Qin Fu(付宝勤), Tun Chen(陈暾), Jie-Chao Cui(崔节超)[†], and Qing Hou(侯氢)[‡]

Key Laboratory of Radiation Physics and Technology of the Ministry of Education, Institute of Nuclear Science and Technology, Sichuan University, Chengdu 610064, *China*

(Received 14 October 2024; revised manuscript received 9 December 2024; accepted manuscript online 8 February 2025)

Nanostructured materials have demonstrated superior radiation-damage tolerance compared to their coarse-grained counterparts, contributing to the extended lifespan of nuclear materials. However, the mechanisms underlying this enhanced irradiation resistance remain unclear. In this study, we present atomistic simulations to investigate the impact of Cu/W heterophase interface on the evolution of irradiation-induced defects. The simulation results reveal that the Cu/W interfaces can act as defect sinks, effectively trapping self-interstitial atoms (SIAs). Furthermore, the interface demonstrates both the interstitial emission and interstitial transfer mechanisms, wherein the trapped W SIAs facilitate the emission of Cu atoms from the interface to the Cu side. These emitted Cu SIAs can promote defect recombination on the Cu side, leading to a reduced defect concentration in the Cu/W nanomultilayers. Consequently, these combined mechanisms contribute to a lower overall concentration of irradiation-induced defect, thereby enhancing the radiation resistance of Cu/W nanomultilayers.

Keywords: molecular dynamics, Cu/W nano-multilayers, interstitial transfer mechanism, radiation resistance

PACS: 61.80.Az, 61.46.–w, 61.72.J–, 02.70.Ns

DOI: 10.1088/1674-1056/adb40d **CSTR:** 32038.14.CPB.adb40d

1. Introduction

Materials employed in nuclear reactors are subjected to high-fluence and high-energy neutron irradiation.[1–3] This results in the generation of a substantial number of Frenkel pairs (FPs), *i.e.* self-interstitial atoms (SIAs) and vacancies.[4,5] Defect accumulation can lead to the degradation of materials' properties. Nanostructured materials[6–12] have garnered considerable interest due to their superior radiation-damage tolerance compared to their coarse-grained counterparts,[13] contributing to the extended lifespan of nuclear materials. This enhanced tolerance is attributed to their extremely high dense grain boundaries (GBs),[6,13] and heterophase interfaces,[14] which effectively absorb and annihilate radiation-induced defects. Such characteristics reduce the concentration of radiation-induced defects, improve swelling resistance, and maintain the morphological stability of multilayered microstructures.[7–10,15] Especially, they preferentially absorb SIAs over vacancies, significantly influencing the radiation resistance of nuclear materials.[16,17]

Besides directly absorbing defects, Bai *et al.*[6] observed that GBs in pure copper (Cu) can re-emit trapped SIAs, allowing them to recombine with nearby vacancies through the interstitial emission (IE) mechanism. Li *et al.*[17] reported on the segregation and annihilation processes of vacancies and SIAs near the GBs. Additionally, Liu *et al.*[14] found that the Cu/niobium (Nb) heterophase interface preferentially traps Cu SIAs rather than Nb SIA, which is subsequently released to recombine with Cu vacancies on the Cu side. These findings highlight the complex interaction between defects and GBs/heterophase interfaces, which plays a crucial role in enhancing radiation-damage tolerance.

Owing to its high thermal conductivity, Cu has emerged as a potential heat sink material for future nuclear fusion reactors.[18] Tungsten (W) is considered a promising plasma-facing material for these reactors because of its exceptional properties, including high melting point, excellent thermal conductivity, and low sputtering yield.[19] Cu/W nanomultilayers[12,15,20] have been proposed as candidate structures for connecting W and Cu in diverters. The crystal structures of Cu and W are distinct; Cu exhibits a face-centered cubic (FCC) configuration, while W adopts a body-centered cubic (BCC) configuration. Theoretically, an incoherent FCC–BCC heterophase interface between Cu and W serves as an effective defect sink,[8,12] significantly influencing the evolution and recovery of radiation-induced defects. Recent experimental studies[9,10,15] on Cu/W nano-multilayers subjected to He ion irradiation have demonstrated remarkable radiation-damage tolerance. These studies indicate that the Cu/W nanomultilayers with smaller period-thickness exhibit stronger radiation resistance, as evidenced by less pronounced changes in

[†]Corresponding author. E-mail: jiechaocui@scu.edu.cn

[‡]Corresponding author. E-mail: qhou@scu.edu.cn

© 2025 Chinese Physical Society and IOP Publishing Ltd. All rights, including for text and data mining, AI training, and similar technologies, are reserved.

interface texture[10] and a lower concentration of vacancy-type defects.[9] However, detailed insights into how heterophase interfaces influence the evolution of irradiation-induced defects and enhance the radiation resistance of Cu/W nano-multilayers remain lacking.

This study aims to address these gaps through molecular dynamics (MD) simulations of Cu/W nano-multilayers. These nano-multilayers possess a polycrystalline structure, with W(110) and Cu(111) serving as the primary diffraction planes.[8,21,22] The Kurdjumov–Sachs[23] (KS) orientation relation at the Cu(111)/W(110) heterophase interface forms the basis for the atomic model used in the simulations. This study investigates the effects of Cu/W heterophase interfaces on the evolution of SIAs and explores the underlying mechanisms that enhance the radiation resistance of Cu/W nano-multilayers.

2. Model and methods

2.1. Simulation model

This study utilizes the graphics processing unit (GPU)-accelerated Molecular Dynamics Package of Sichuan University (MDPSCU)[24] to conduct MD simulations. The embedded atom method (EAM) interatomic potential developed by Zhou *et al.*[25] is employed for simulating the Cu–W systems. This potential has demonstrated its reliability in various atomic simulation studies.[12,21,26]

Figure 1 displays the prepared Cu/W nano-multilayers simulation box. Previous researches[11,21] have shown that the mismatch between two metals affects their interaction. Thus, simulations require a minimal mismatch for accuracy and representation. Thus, in this study, the Cu/W simulation box is constructed by joining the Cu with the W simulation boxes, ensuring a mismatch of less than 0.058%. Periodic boundary conditions are applied in all three directions. Table 1 lists the computed parameters for the simulation box.

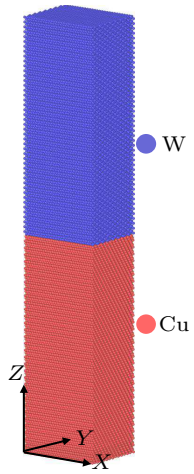


Fig. 1. Initial configuration of Cu/W nano-multilayers.

Table 1. Computed parameters of the initial simulation box. L_x, L_y, and L_z are the lengths along the x, y, and z directions, respectively.

Material type	$L_x \times L_y \times L_z/(a_0^{\mathrm{Cu}})^3$	x direction	y direction	z direction	Total atoms
Cu/W nano-multilayers	17.15×21.21×111.38	$[1\bar{1}0]_{\mathrm{Cu}}\|\|[\bar{1}11]_{\mathrm{W}}$	$[11\bar{2}]_{\mathrm{Cu}}\|\|[1\bar{1}2]_{\mathrm{W}}$	$[111]_{\mathrm{Cu}}\|\|[110]_{\mathrm{W}}$	141120

The lattice length a_0^{Cu} of Cu is initially set to be 3.615 Å. For convenience, the lattice length of W (3.165 Å) is expressed as $0.87552a_0^{\mathrm{Cu}}$. Considering the lattice mismatch between Cu and W, as well as the undetermined distance between Cu and W interfaces in the Cu/W model,[11,21] we adjust a_0^{Cu} from 3.603 Å to 3.627 Å (12 data points) to identify the stable state of the Cu/W model. Cu/W nano-multilayers can serve as joining materials for plasma-facing materials (W) and heat sink materials (Cu) with operating temperatures ranging from 450 K to 1050 K.[27–29] Therefore, the simulation system is then thermalized to 700 K by assigning the atomic velocities according to the Maxwell distribution. Subsequently, the system is subjected to an NVT ensemble, simulating for approximately 500 ps at 700 K to achieve stable interface structures, before being quenched to 0 K. We employ the gradient descent method to minimize the system's energy and calculate the potential energy versus lattice length curve. Using the least squares method, we fit the data points with a cubic polynomial to model this curve. Subsequently, Newton's optimization method is applied to determine the minimum energy point on the fitted curve, yielding a corresponding a_0^{Cu} value 3.61446 Å. This approach ensures that the simulation box could attain its most stable or ground state after thermodynamic relaxation.

2.2. Calculation of SIA–Cu/W heterophase interface interaction

To explore the underlying mechanisms by which Cu/W heterophase interfaces enhance radiation resistance, we initially examine the evolution of the Cu/W heterophase interface as it continuously traps Cu or W SIAs. Specifically, the Cu (W) SIAs are inserted into the system containing Cu/W interface in an accumulative pattern. The SIAs are randomly positioned within the first three Cu monolayers (for Cu SIAs) and two W monolayers (for W SIAs) along the interface. In this region, the interface exhibits a strong absorption for SIAs (Fig. 6(a)). After each insertion, the system is firstly quenched to 0 K, then thermalized to 700 K, and subsequently allowed to evolve freely for approximately 40 ps. This duration is sufficient for the SIA to be absorbed by the interface. In total, 160 Cu (W) SIAs are inserted into the system.

To further compare the influence of Cu and W SIAs on Cu/W interface, 160 Cu SIAs and 160 W SIAs are introduced simultaneously into one system. During each introduction step, one Cu SIA and one W SIA are inserted together. The Cu SIAs are still placed within the first three Cu monolayers along the interface, while the W SIAs are positioned within the first two W monolayers. Other simulation details remain the same as previously described. The structural evolution of the nano-multilayer system after quenching to 0 K was tracked using common neighbor analysis (CNA).[30] implemented in OVITO.[31]

We also calculate the formation energies of single SIAs at various locations to explore their interactions with the interface. This analysis involves uniformly and randomly introducing a single Cu (W) SIA into the Cu (W) side of the Cu/W model. To reduce statistical errors, a total of 1700 independent simulation boxes are used (800 boxes for single Cu SIAs and 900 boxes for single W SIAs). After the introduction, the systems are quenched to 0 K, and the distribution of the SIAs is subsequently analyzed. The interstitial formation energy E_{f} is given by[12]

$$E_{\mathrm{f}} = E_{\mathrm{SIA-int}} - E_{\mathrm{int}} - E_{\mathrm{coh}}, \tag{1}$$

where $E_{\mathrm{SIA-int}}$ is the total energy of the Cu/W system containing a defect induced by the insertion of a single Cu or W SIA, E_{coh} represents the cohesive energy of a Cu or W atom in the bulk, and E_{int} is the total energy of the Cu/W system without defects.

3. Simulation results

3.1. Response of Cu/W heterophase interface to loaded SIAs

Considering the roles of GBs in pure Cu[6,32] and W,[33] the Cu/W heterophase interface[9,10,34] may also exhibit a distinct IE mechanism[6,14] for mitigating radiation damage.

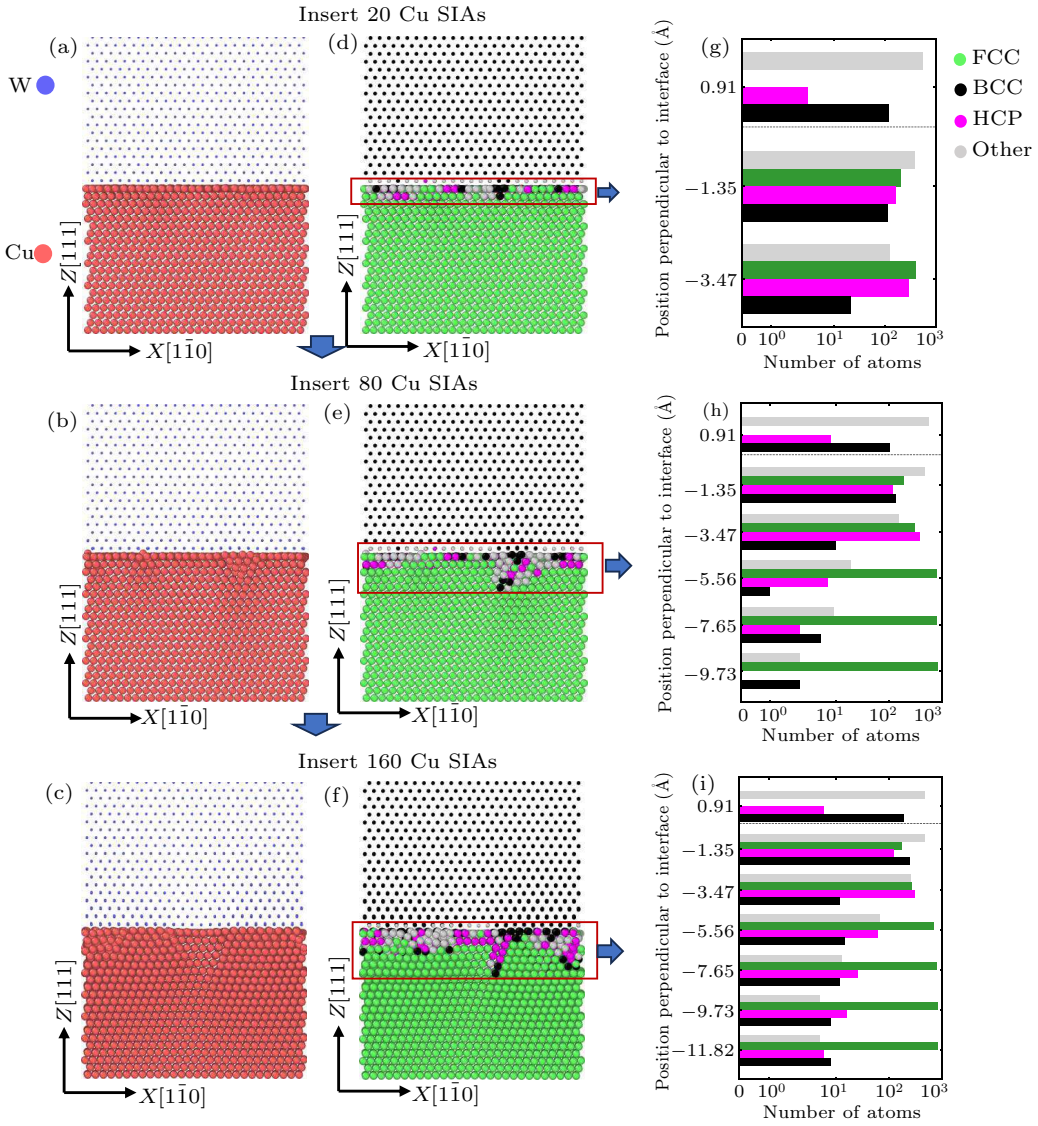


Fig. 2. Evolution of the Cu/W model with the introduction of Cu SIAs. (a)–(c) Atomic configurations, (d)–(f) crystal structures, (g)–(i) distributions of the atoms with different crystal structures corresponding to the region enclosed by red lines in panels (d)–(f). The blue and red spheres in panels (a)–(c) represent W and Cu atoms, respectively. The dotted line in panels (d)–(f) indicates the interface.

To explore this possibility, we investigate the evolution of the interface after trapping Cu SIAs, W SIAs, and a mixture of both. Figure 2 illustrates the evolution of the interface as it continuously absorbs Cu SIAs. As shown in Figs. 2(a)–2(c), Cu SIAs trapped by the interface remain on the Cu side. As more Cu SIAs are trapped, the interfacial Cu plane becomes disordered, leading to an increase in non-FCC Cu atoms that grow towards the Cu side along the interfacial Cu plane (Figs. 2(d)–2(i)). Conversely, there is no significant alteration in the atomic configurations on the W side. These results indicate that the IE mechanism indeed plays a role when the interface traps Cu SIAs.

However, the situation is different when the interface traps W SIAs. The evolution of the interface as it continuously absorbs W SIAs is presented in Fig. 3. Unlike the observations in Figs. 2(a)–2(c), where Cu SIAs are introduced, the insertion of W SIAs on the W side does not lead to any obvious alteration in the structure and atomic configurations of the W side (Figs. 3(a)–3(f)). On the contrary, W SIAs trapped by the interface migrate from the W side to the Cu side, as shown in Figs. 3(a)–3(c). These trapped W SIAs adopt a BCC configuration, displacing Cu atoms from their original positions, which facilitates the emission of Cu atoms from the interface to the Cu side. As more W SIAs are trapped, the number of non-FCC atoms increases, growing towards the Cu side along the interfacial Cu plane (Figs. 3(d)–3(f)). This behavior contrasts with the IE mechanism reported in Refs. [6,14,17]. Instead, the Cu/W heterophase interface exhibits an interstitial transfer (IT) mechanism, where interface-trapped W SIAs can facilitate the emission of Cu atoms from the interface to the Cu side.

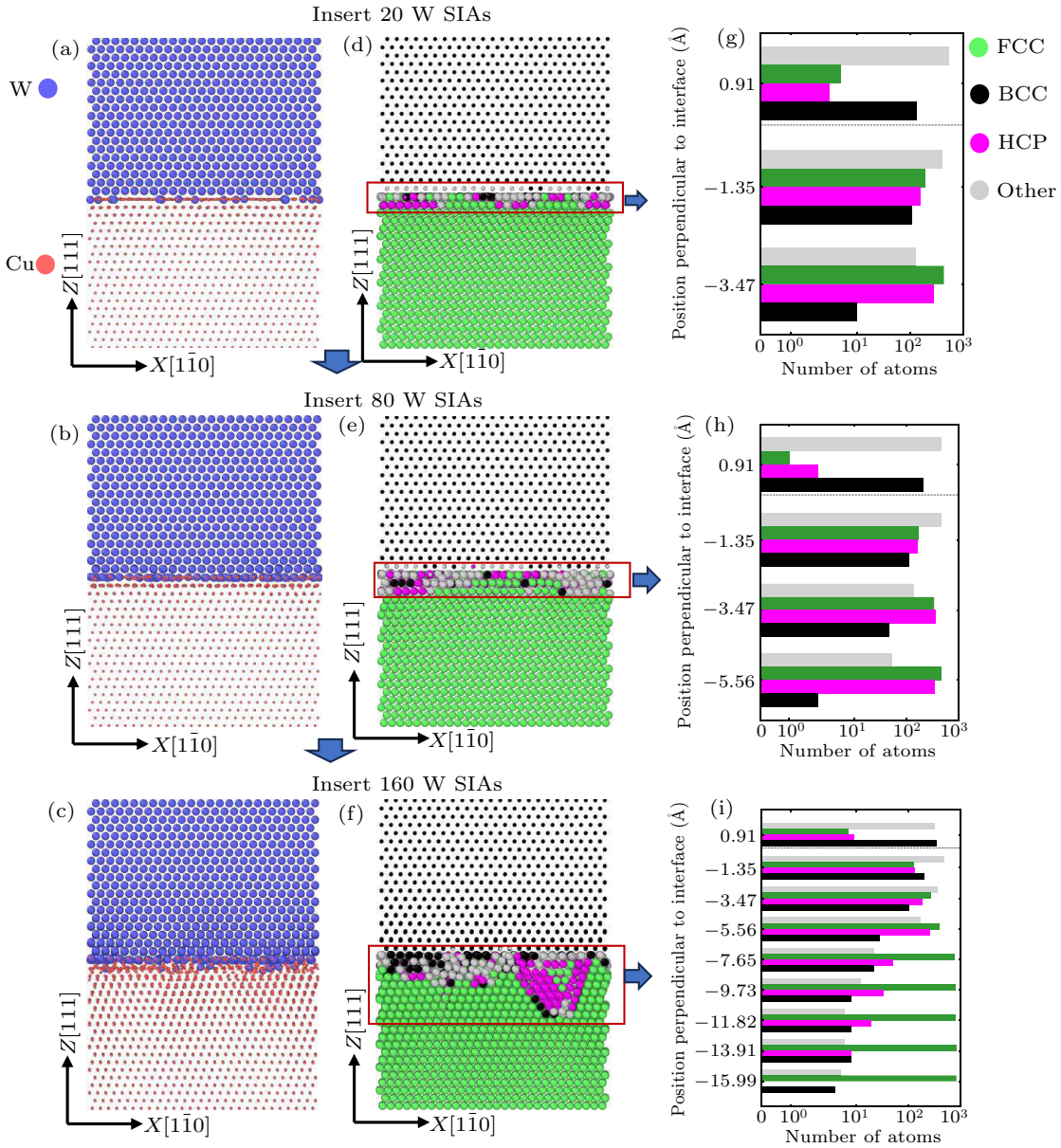


Fig. 3. Evolution of the Cu/W model with the introduction of W SIAs. (a)–(c) Atomic configurations, (d)–(f) crystal structures, (g)–(i) distributions of the atoms with different crystal structures corresponding to the region enclosed by red lines in panels (d)–(f). The blue and red spheres in panels (a)–(c) represent W and Cu atoms, respectively. The dotted line in panels (d)–(f) indicates the interface.

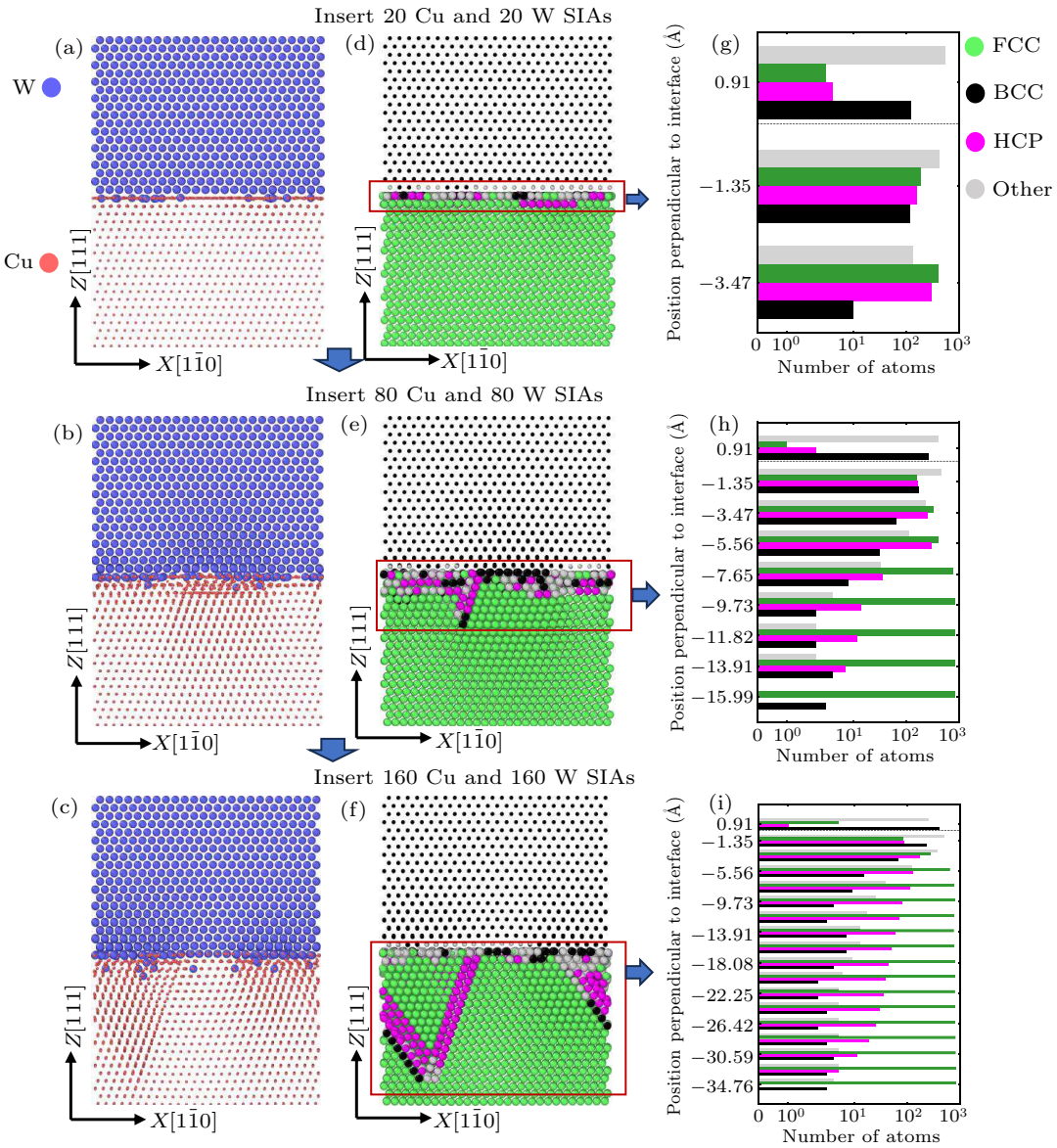


Fig. 4. Evolution of the Cu/W model with the simultaneous introduction of Cu and SIAs. (a)–(c) Atomic configurations, (d)–(f) crystal structures, (g)–(i) distributions of the atoms with different crystal structures corresponding to the region enclosed by red lines in panels (d)–(f). The blue and red spheres in panels (a)–(c) represent W and Cu atoms, respectively. The dotted line in panels (d)–(f) indicates the interface.

It seems that inserting 160 W SIAs on the W side causes more severe damage to the adjacent Cu layer than inserting the same number of Cu SIAs on the Cu side, as shown in Figs. 2 and 3. To further compare the influence of Cu and W SIAs on Cu/W interface, Cu SIAs and W SIAs are introduced simultaneously into a single simulation box. Figure 4 presents the results. All Cu SIAs remain on the Cu side, while the W SIAs continue to migrate from the W side to the Cu side, similar to the result shown in Fig. 3. Consequently, compared to the results from the previous two simulations (Figs. 2 and 3), significant structure deformation also occurs on the Cu side and more non-FCC atoms appear. This phenomenon indicates that the IT and IE mechanisms can work synergistically when the interface simultaneously traps W SIAs and Cu SIAs. The predominant deformation on the Cu side is consistent with observations made when the Cu/W heterophase interface is subjected to tensile loading.[26,35] This behavior can be attributed to Cu's relatively lower mechanical strength compared to W, leading to the presence of Cu/W interface greatly weakening the deformability of Cu.[26]

Figure 5 displays the atomic configurations of the Cu (Figs. 5(a)–5(c)) and W (Figs. 5(d)–5(f)) layers along the interface when the interface simultaneously traps W SIAs and Cu SIAs. As shown in Figs. 5(a) and 5(d), the initial atomic structures of the interface exhibit a regular arrangement pattern, similar to phenomena reported in Refs. [12,22,36]. This regular pattern is associated with the in-plane array of misfit dislocation nucleates, which serve as geometrically favorable sites for dislocation emission.[26,36–39] As shown in Figs. 5(a)–5(c), the increasing number of trapped Cu and W SIAs disrupts this regular arrangement pattern. Non-FCC atoms and Shockley partial dislocations proliferate along the interfacial Cu plane and extend toward the Cu side. In contrast, although BCC W atoms also proliferate along the interfacial W plane,

the W plane remains flat (Figs. 5(d)–5(f)). These observations are consistent with the findings in Figs. 2–4. As trapped SIAs cause a transformation from the regular arrangement pattern to a distorted pattern in the interface structure, the emission locations of Shockley partial dislocations and the growth of non-FCC atoms become decoupled from the initial atomic structures of the interface. This differs from the findings reported in Refs. [26,36].

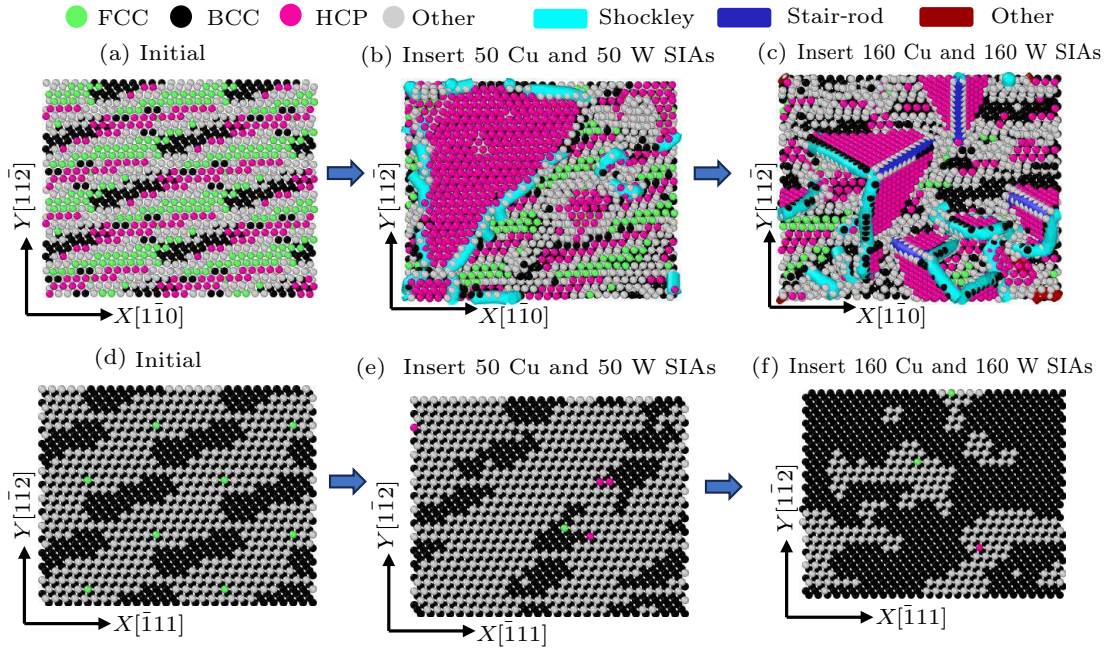


Fig. 5. Atomic configurations of (a)–(c) Cu and (d)–(f) W layers along the interface.

3.2. Investigation of IT mechanism

The W SIA-loaded Cu/W heterophase interface triggers the IT mechanism, rather than the more commonly recognized IE mechanism. Therefore, gaining further insight into this IT mechanism is essential. We investigate the interactions between single SIAs and the interface. As noted in Subsection 2.2, all independent simulation boxes are ultimately quenched to 0 K. The final positions of defects induced by the inserted SIAs are determined using Wigner–Seitz (WS) defect analysis.[40] The identified defects include Cu SIAs, W SIAs, and combined Cu–W combinations. A Cu–W combination contains a BCC W and a Cu SIAs. Thus, it reflects the growth of BCC W toward the Cu side. Figure 6 illustrates the distribution of these defects. As indicated by the region enclosed by red dashed lines in Fig. 6(a), after inserting Cu SIAs, the defect concentration within the first atomic layer on the Cu side is considerably higher than that in the second to fourth atomic layers near the interface. Conversely, no defects are observed within the first atomic layer on the W side when inserting W SIAs; instead, some migrate to the Cu side (green spheres). The green spheres in Fig. 6(b) represent two types of W atoms, which help explain the phenomenon observed in Fig. 6(a). The first type consists of W atoms that have combined with neighboring Cu atoms, forming Cu–W combinations. The second type includes W atoms that facilitate the emission of Cu SIAs. Thus, even single W atoms trapped by the interface (green spheres) could promote Cu emission from the interface to the Cu side (cyan spheres), albeit with a very low probability. This finding is consistent with the results shown in Figs. 2–4. Therefore, while substantial absorption occurs when all SIAs migrate near the interface, the interface's influence on Cu SIAs extends further than that on W SIAs.

Based on the quenched simulation boxes, we calculate the average interstitial formation energy E_f of defects induced by inserted Cu SIAs (Fig. 7(a)) and W SIAs (Fig. 7(b)). The results show that the E_f of individual Cu and W SIAs within the bulk are approximately 3.15 eV and 9.72 eV, respectively. Notably, the E_f for a single Cu SIA significantly decreases to 1.47 eV (Fig. 7(a)) near the interface. In contrast, a single W SIA cannot exist near the interface. Using WS defect analysis and visualization tools implemented in OVITO, we observe that when inserting W SIAs, the defects in the first layer on the Cu side, indicated by the green square in Fig. 7(b), are Cu–W combinations with $E_f = 2.06$ eV. Additionally, single Cu SIAs emitted as a result of W SIA insertion are identified in the second to third atomic layers away from the interface (in the region enclosed by cyan lines), with formation energies of 3.46 eV and 3.7 eV, respectively. This phenomenon can be attributed to the absorption of single W atoms by the interface, which leads to the emission of a single Cu SIA toward the Cu side (denoted by the left insert of Fig. 7(b)), consistent with the observations in Fig. 6(b).

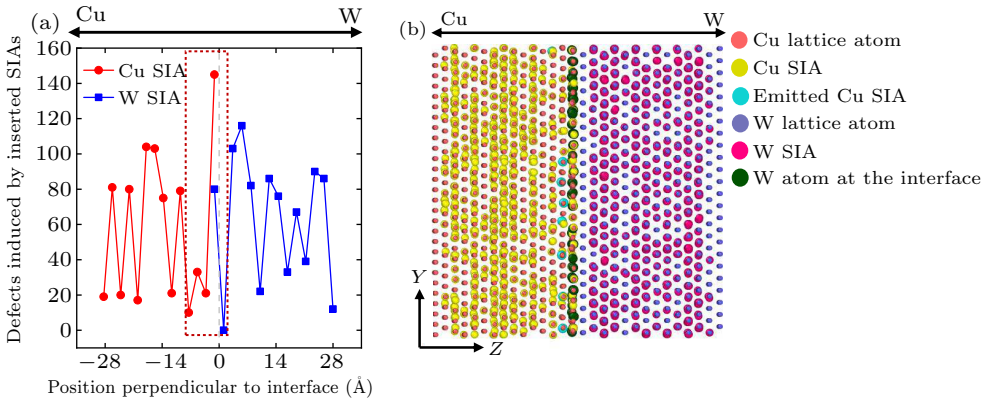


Fig. 6. (a) Distance between the defects induced by inserted SIAs and Cu/W heterophase interface after relaxation. The region enclosed by the red dashed lines indicates that Cu and W atoms are trapped at the interface at 0 K. (b) Position distribution of defects in 1700 simulation boxes.

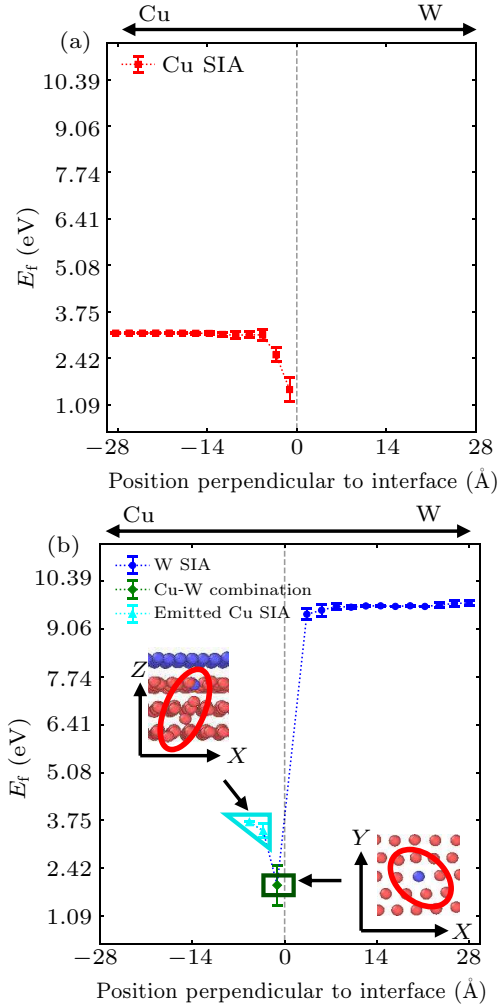


Fig. 7. The average interstitial formation energy E_f of defects induced by inserted (a) Cu SIAs and (b) W SIAs in Cu/W simulation box. The box was relaxed at 0 K. The data are averaged over bins with a width equal to half the sum of the distances between the intermediate and two neighboring atomic layers. The standard deviation indicates the extent to which the formation energy of a defect deviates from the average formation energy of defects. The cyan triangular and green squares in panel (b) correspond to the emitted Cu SIAs and part of the Cu–W combinations in Fig. 6(b), respectively.

We further investigate how a single trapped W SIA facilitates the emission of a Cu SIA to the Cu side and the recombination of Cu SIA with vacancy. As shown in Figs. 8(a) and 8(b), when a single W SIA migrates close to the interface and becomes trapped, it directly displaces Cu atoms along its migration path, leading to the emission of a Cu SIA toward the Cu side. Subsequently, the emitted Cu SIA moves toward the Cu vacancy at the third atomic layer near the interface and recombines with it (Figs. 8(c) and 8(d)).

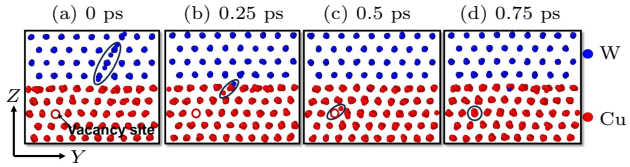


Fig. 8. Emission and annihilation of Cu SIA. (a) At the interface, the trapped W atom displaces the Cu atoms, leading to the emission of a Cu SIA toward the Cu side; (b)–(c) the emitted Cu SIA moves towards the Cu vacancy at the third atomic layer near the interface; (d) Cu SIA recombines with the Cu vacancy.

4. Discussion

Radiation damage in Cu/W single crystal leads to the generation of numerous FPs, specifically SIAs and vacancies. SIAs can immediately recombine with nearby vacancies upon thermal activation.[41,42] In contrast, Cu SIAs and W SIAs that are further away from vacancies migrate freely.[41] These mobile SIAs not only recombine with other vacancies but also cluster with additional SIA-type defects, forming larger SIA clusters, such as dislocation loops. Additionally, they migrate to surfaces, contributing to the formation of new layers.[43–45] Meanwhile, vacancies migrate and aggregate, leading to the formation of vacancy clusters, such as voids.[32,42,43] The continuous microstructural changes due to radiation damage contribute to material deterioration, significantly shortening the lifespan of nuclear materials.

Here, we explore how Cu/W nano-multilayers influence the evolution of irradiation-induced defects, focusing on the critical role of SIA migration. In Cu/W nano-multilayers, both Cu and W SIAs can be trapped by Cu/W heterophase interfaces. Once trapped, these atoms tend to accumulate on the interfacial Cu plane, resulting in the growth of non-FCC atoms, predominantly on the Cu side (Figs. 2 and 3). The SIA-loaded Cu/W heterophase interface demonstrates two distinct mech-

anisms: the IE mechanism and the IT mechanism. In the IT mechanism, the trapped W SIAs can facilitate the emission of Cu atoms from the interface to the Cu side, even in the absence of Cu vacancies near the interface and Cu SIAs at the interface (Fig. 3). This behavior contrasts with that observed at the Cu/Nb heterophase interface, where Cu SIAs[14] are preferentially trapped and subsequently released to the Cu side, rather than Nb SIAs. Both the IE and IT mechanisms promote the emission of Cu SIAs from the interface and facilitate recombination with vacancies on the Cu side.

Therefore, multiple mechanisms enhance the radiation resistance of Cu/W nano-multilayers. First, the interface absorbs defects, especially SIAs, resulting in reduced irradiation-induced defects within the bulk. Second, the interfaces favor the recombination of defects on the Cu side through the IE and IT mechanisms. Consequently, the overall irradiation-induced defect concentration is lowered.

5. Conclusions

Atomistic simulations are conducted to investigate the influence of Cu/W heterophase interface on the evolution of irradiation-induced defects. The simulation results reveal that the interface serve as a defect sink, effectively trapping SIAs. The SIA-loaded interface demonstrated two mechanisms for inducing the emission of Cu atoms from the interface to the Cu side: the IE mechanism and the IT mechanism. The IE mechanism occurs when the interface traps Cu SIAs, while the IT mechanism, plays a role when the interface traps W SIAs. Both mechanisms facilitate defect recombination, contributing to the enhanced radiation resistance of Cu/W nano-multilayers.

Acknowledgements

Project supported by the National Natural Science Foundation of China (Grant No. 12105194) and the Natural Science Foundation of Sichuan Province of China (Grant Nos. 2022NSFSC1251 and 2022NSFSC1265).

References

[1] Hasegawa A, Fukuda M, Nogami S and Yabuuchi K 2014 *Fusion Eng. Des.* **89** 1568
[2] Hasegawa A, Fukuda M, Yabuuchi K and Nogami S 2016 *J. Nucl. Mater.* **471** 175
[3] Fukuda M, Tanno T, Nogami S and Hasegawa A 2012 *Mater. Trans.* **53** 2145
[4] Cui J C, Zhou Z B, Fu B Q and Hou Q 2020 *Nucl. Instrum. Methods Phys. Res. Sect. B Beam Interact. Mater. At.* **471** 90
[5] Jiang L, Li M, Fu B Q, Cui J C and Hou Q 2024 *Chin. Phys. B* **33** 036103
[6] Bai X M, Voter A F, Hoagland R G, Nastasi M and Uberuaga B P 2010 *Science* **327** 1631
[7] Beyerlein I J, Caro A, Demkowicz M J, Mara N A, Misra A and Uberuaga B P 2013 *Mater. Today* **16** 443
[8] Callisti M, Karlik M and Polcar T 2016 *J. Nucl. Mater.* **473** 18
[9] Chen H C, Hai Y, Zhan X Z, Xu J P, Cao X Z, Zhu T and Yin W 2022 *Crystals* **12** 759
[10] Gao Y, Yang T F, Xue J M, Yan S, Zhou S Q, Wang Y Q, Kwok D T K, Chu P K and Zhang Y W 2011 *J. Nucl. Mater.* **413** 11
[11] González C and Iglesias R 2016 *Mater. Des.* **91** 171
[12] Li M, Hou Q, Cui J, Qiu M, Yang A and Zhou M 2021 *J. Nucl. Mater.* **555** 153157
[13] Bai X M and Uberuaga B P 2013 *Jom* **65** 360
[14] Liu X Y, Uberuaga B P, Demkowicz M J, Germann T C, Misra A and Nastasi M 2012 *Phys. Rev. B* **85** 012103
[15] Dong L, Zhang H, Amekura H, Ren F, Chettah A, Hong M, Qin W, Tang J, Hu L, Wang H and Jiang C 2017 *J. Nucl. Mater.* **497** 117
[16] Han W, Demkowicz M J, Mara N A, Fu E, Sinha S, Rollett A D, Wang Y, Carpenter J S, Beyerlein I J and Misra A 2013 *Adv. Mater.* **25** 6975
[17] Li X, Liu W, Xu Y, Liu C S, Pan B C, Liang Y, Fang Q F, Chen J L, Luo G N, Lu G H and Wang Z 2016 *Acta Mater.* **109** 115
[18] Fabritsiev S A, Zinkle S J and Singh B N 1996 *J. Nucl. Mater.* **233** 127
[19] Tanno T, Fukuda M, Nogami S and Hasegawa A 2011 *Mater. Trans.* **52** 1447
[20] Pintsuk G, Brünings S E, Döring J E, Linke J, Smid I and Xue L 2003 *Fusion Eng. Des.* **66** 237
[21] Bodlos R, Fotopoulos V, Spitaler J, Shluger A L and Romaner L 2022 *Materialia* **21** 101362
[22] Demkowicz M J, Hoagland R G and Hirth J P 2008 *Phys. Rev. Lett.* **100** 136102
[23] Kurdjumow G and Sachs G 1930 *Z. Für Phys.* **64** 325
[24] Hou Q, Li M, Zhou Y L, Cui J C, Cui Z G and Wang J 2013 *Comput. Phys. Commun.* **184** 2091
[25] Zhou X W, Johnson R A and Wadley H N G 2004 *Phys. Rev. B* **69** 144113
[26] Ma G C, Fan J L and Gong H R 2018 *Comput. Mater. Sci.* **152** 165
[27] Huang Y, Sun J, Ding R, Sang C and Wang D 2023 *Fusion Eng. Des.* **192** 113824
[28] Li C, Zhu D, Ding R, Wang B, Chen J, Gao B and Lei Y 2020 *Nucl. Mater. Energy* **25** 100847
[29] Poleshchuk K, Terentyev D, Galatanu A and Verbeken K 2025 *J. Nucl. Mater.* **604** 155496
[30] Larsen P M 2020 *ArXiv Comput. Phys.*
[31] Stukowski A 2010 *Model. Simul. Mater. Sci. Eng.* **18** 015012
[32] Jin M M, Cao P H, Yip S and Short M P 2018 *Acta Mater.* **155** 410
[33] Li X Y, Liu W, Xu Y C, Liu C S, Fang Q F, Pan B C, Chen J L, Luo G N and Wang Z G 2013 *Nucl. Fusion* **53** 123014
[34] Chen F D, Tang X B, Yang Y H, Huang H, Liu J, Li H and Chen D 2016 *J. Nucl. Mater.* **468** 164
[35] Chen X, Xie Y and Huang Y 2023 *J. Mol. Model.* **29** 247
[36] Zhang R F, Germann T C, Wang J, Liu X Y and Beyerlein I J 2013 *Scr. Mater.* **68** 114
[37] Zhang R F, Wang J, Beyerlein I J and Germann T C 2011 *Scr. Mater.* **65** 1022
[38] Mara N A and Beyerlein I J 2014 *J. Mater. Sci.* **49** 6497
[39] Beyerlein I J, Mara N A, Wang J, Carpenter J S, Zheng S J, Han W Z, Zhang R F, Kang K, Nizolek T and Pollock T M 2012 *Jom* **64** 1192
[40] Tanemura M, Ogawa T and Ogita N 1983 *J. Comput. Phys.* **51** 191
[41] Schilling W and Sonnenberg K 1973 *J. Phys. F-Met. Phys.* **3** 322
[42] Eyre B L 1973 *J. Phys. F Met. Phys.* **3** 422
[43] Gilbert M R, Arakawa K, Bergstrom Z, *et al.* 2021 *J. Nucl. Mater.* **554** 153113
[44] Jourdan T and Nastar M 2022 *J. Appl. Phys.* **131** 225103
[45] Mason D R, Das S, Derlet P M, Dudarev S L, London A J, Yu H B, Phillips N W, Yang D, Mizohata K, Xu R Q and Hofmann F 2020 *Phys. Rev. Lett.* **125** 225503